

CREEP BEHAVIOR OF AN EQUIMOLAR CONIFEMNCR HIGH ENTROPY ALLOY AT 1000°C AND BEYOND

Patrice BERTHOD^{1,*} [0000-0002-8035-927X]

¹ Faculté des Sciences et Technologies & Institut Jean Lamour,
Université de Lorraine, 2 allée André Guinier 54000 Nancy, France

Abstract

The Cantor alloy is one of the earliest high entropy alloys to appear. In contrast with its properties at low and cryogenic temperatures, its creep behavior at close to 1000°C is not yet very known. This work aims to explore the behavior of a cast equimolar CoNiFeMnCr alloy in three points bending creep at 1000 and 1100°C for two levels of loading (inducing 10 and 30 MPa tensile stress). The deformation rate increases with temperature and with stress. Duration to test end can reach 100 hours and more for 10 MPa and 50h or much less for 30 MPa. In addition, significant oxidation of the samples was noticed by oxygen impurities in the protective argon atmosphere. These results demonstrate that, in its present state, this alloy is not suitable for service at so high temperature. It must be mechanically strengthened, by precipitates for instance, and its oxidation resistance must be improved.

Keywords: *equimolar CoNiFeMnCr alloy, high temperature creep, high temperature oxidation.*

Introduction

Superalloys are, for most of them, rich in either nickel or in cobalt, in these two elements simultaneously in some cases [1]. The weight contents in Ni and/or Co are frequently higher than 60 wt.%. These base elements cause more and more problems of availability and various ways are exploited to recover/collect Ni and Co [2,3]. Decreasing the Ni and Co contents in superalloys by limited replacement by other elements such as Fe is a solution to be less dependent on Ni and Co supply. This may lead to chemical compositions close to some High Entropy Alloys [4], among them the Cantor's alloy [5] and other early HEAs [6]. The challenge of such composition changes is thus ensuring the manufacturing sustainability, and this without loss of high temperature properties for maintaining service lifetime at a still acceptable level, if possible comparable to the superalloy's ones. Knowing the high temperature performances of the Cantor's alloy, alloy associating Co, Ni, Fe, Mn and Cr in similar contents and thus which may look like superalloys with less Ni or Co and containing Fe and Mn instead, is consequently of great interest. The mechanical behavior must be particularly anticipated since it is only dependent on the bulk material, while eventual problems of hot oxidation/corrosion can be solved by applying protective coatings. The Cantor's alloy, as well as its subsets [7] and derivatives [8–10], has been till today extensively studied. Most of investigations carried out for characterizing the mechanical behavior of Cantor-type alloys concerned only tests carried out at low temperatures ([11, 12] for instance). The tests performed for exploring the mechanical behavior of this alloy were performed for various types of mechanical solicitation: traction (e.g. [13]) and compression (e.g. [14]) for static

loading, alternative uniaxial tensile–compressive dynamic loading for fatigue tests (e.g. [15])... Cantor–type alloys were also tested in uniaxial loading at more than room temperatures but only up to temperatures equal or close to 650°C–700°C ([17–21]. The highest test temperatures for mechanical testing which can be found in published works were 1050–1100°C, and this was in compression [22] and in torsion [23]. One must also notice a work dealing with the tensile behavior of the Cantor’s alloy at 1100°C but for a single–crystalline one [24], thus an alloy not weakened by grain boundaries as a polycrystalline equi–axed Cantor alloy.

Thus, it seems that the Cantor’s alloy, to which the superalloys compositions may converge by decreasing the Ni and Co contents thanks to their partial replacement by much less strategic metals such as Fe and Mn, is not very known today concerning its tensile and flexural behaviors at elevated temperature. There is a lack of behavior knowledge for the {tensile creep, 1000 to 1100°C} and {flexural creep, 1000 to 1100°C} combinations of conditions of test. This is problematic since the metallic components used in the hottest parts of machines/production facilities working at high temperature are principally exposed to tensile and flexural solicitations, particularly the turbine blades present in the aeronautical or power generation turbines which usually work at 1000°C to 1100°C. There is thus a potential need of supplemental data concerning the behavior of equimolar CoNiFeMnCr alloys for such working conditions. This is what motivated the present work devoted to the flexural creep resistance of the Cantor alloy.

Material and Methods

A foundry version of the Cantor’s alloy was cast by induction heating under inert atmosphere. Initially, pure Co, Ni, Fe, Mn and Cr parts (for each purity higher than 99.9%) were prepared in quantities controlled using a precision balance ($\pm 10^{-4}$ g) to obtain a total mass equal to forty grams with an elemental repartition corresponding to 20 at.% for each element. In the high frequency induction furnace, the mix of solid parts was heated – under 0.3 bars of Argon – to reach about 1600°C. Melting was followed by an iso-power stage allowing temperature staying around 1600°C for completing fusion and liquid chemical homogenization, during 15 minutes. The solidified ingot was embedded in a resin mixture rigidifying at room temperature with a cylindrical shape to facilitate machining with the metallographic saw. Cutting led to parallelepipeds with dimensions close to the following values: 15 mm (length), 2 mm (width) and 1 mm (thickness). For each specimen width and thickness were accurately determined for the calculation of the exact load to apply for inducing the targeted tensile stresses.

The parallelepiped specimen was supported by two cylindrical Al₂O₃ parallel rods (separated by 12 mm). An-other Al₂O₃ rod, an extremity of which was carved to produce a “V” shape, was placed on the top face of the parallelepiped specimen (three points flexural loading configuration). This third alumina rod, attached to a precision sensor, was both the loading media and the displacement measuring device. Tensile stress equal to 10 MPa or 30 MPa were induced in the middle of the bottom face of the specimen, by loading rated to values taking into account its exact width and thickness. The load was constantly applied all along the creep test, during which a 2 L/min (linear speed: 1.6 mm/s) continuous flow of industrial pure argon (but containing 10 ppm oxygen impurities) protected the most possible the alloy from oxidation. The chosen constant temperatures were 1000°C and 1100°C for the two levels of loading/induced tensile stress. The initial duration of the isothermal creep was 150 hours. It was either extended (slow deformation) or shortened (fast deformation and contact with the alumina base), depending on the specimen behavior.

At the end of the tests, the crept specimens were embedded in resin and ground then polished, to obtain metallographic samples for post-test examination using a scanning electron microscope (SEM): eventual presence of more or less long cracks, of oxides... The later ones were further identified by performing Energy Dispersion Spectrometry analyses (EDS).

Results

Control of the obtained alloy

A metallographic sample prepared from the solidified ingot was characterized by SEM exploration of the internal structure and by EDS measurement of the chemical composition. This confirmed that the alloy was well single-phased and that the targeted chemical composition was effectively obtained. No pertinent micrograph can be shown because of the lack of contrast resulting from the presence of one phase only. In contrast the obtained chemical composition is given in Table 1.

Table 1. Chemical composition of the as-cast alloy (from five $\times 250$ full frame EDS analyses)

At.%	Co	Ni	Fe	Mn	Cr
Average content	19	20	20	20	21
Standard deviation	± 1				

Deformation curves

The obtained deformation curves are plotted in Fig. 1 (under 10 MPa at 1000°C and at 1100°C) and in Fig. 2 (under 30 MPa at 1000°C and 1100°C). Three of the four curves present a plateau as final part, due to the contact of the specimen bottom with the base. This maximal possible deformation was achieved after 100 hours for the {10 MPa, 1100°C} conditions, and sooner for the two other couples of conditions {30 MPa, 1000°C} (≈ 50 hours) and {30 MPa, 1100°C} (≈ 5 hours). {10MPa, 1000°C} was the single couple of conditions for which the deformation rate was acceptable for real service.

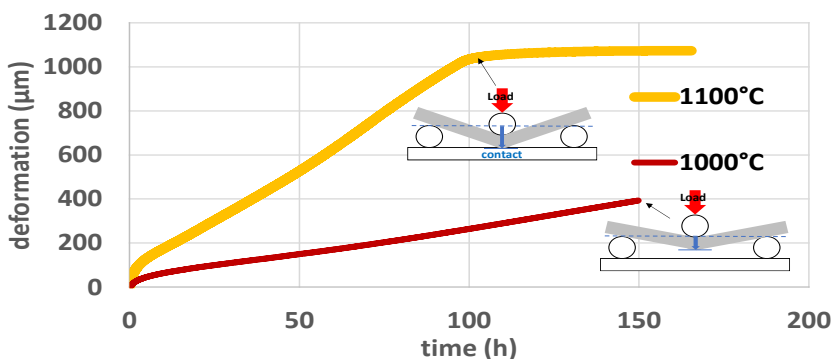


Fig. 1. The two deformation curves obtained for 10 MPa at 1000°C and at 1100°C

This test was interrupted at 150 hours when creep was still in the steady state regime. It can be expected that the duration to contact with the base can be obtained after three times this duration, as is to say between 400 and 500 hours. The primary stage of creep, probably started before that temperature reached the targeted isothermal stage temperature (either 1000 or 1100°C), was in all cases followed by the steady state creep regime (deformation linear versus time). The constant deformation rates were measured on the linear part of the curves. The results, presented in Table 2. Clearly, an crease in induced stress or in temperature lead to accelerated deformation in the secondary stage of creep.

Final states of the crept specimens

After creep test and return to room temperature, the crept specimen were photographed. After embedding in cold resin, grinding and polishing, they were examined using the SEM. The

photographs and the some of the SEM images are presented in Fig. 3, Fig. 4, Fig. 5 and Fig. 6, for the {10 MPa, 1000°C}, {10 MPa, 1100°C}, {30 MPa, 1000°C} and {30 MPa, 1100°C} couples of creep test conditions, respectively. The two thick specimen deformed under 10 MPa, for which the creep durations were the longest (100h until contact with base or 150h before test interruption) are the most affected by cavitation (high densities of pores) and cracks. The two other specimens (thinner than the former ones, deformed under 30 MPa) contain less porosities and cracks. One can also notice that all specimens were oxidized, this demonstrating that the pure argon flow was not protective.

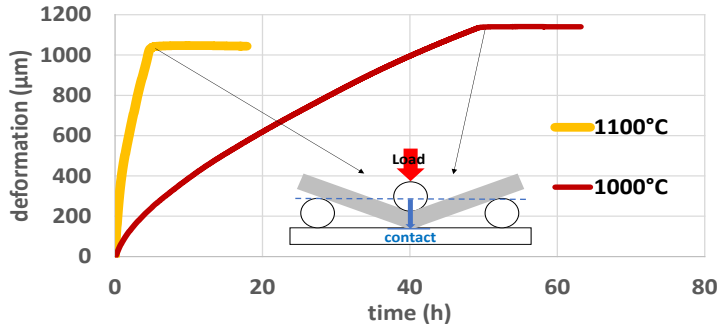


Fig. 2. The two deformation curves obtained for 30 MPa at 1000°C and at 1100°C

Table 2. Values of the steady state deformation rate for the four { σ , T} couples of conditions

Induced tensile stress (σ)	Isothermal stage temperature (T)	Steady state deformation rate
10 MPa	1000°C	2.4 $\mu\text{m/h}$
10 MPa	1100°C	9.9 $\mu\text{m/h}$
30 MPa	1000°C	18 $\mu\text{m/h}$
30 MPa	1100°C	157 $\mu\text{m/h}$

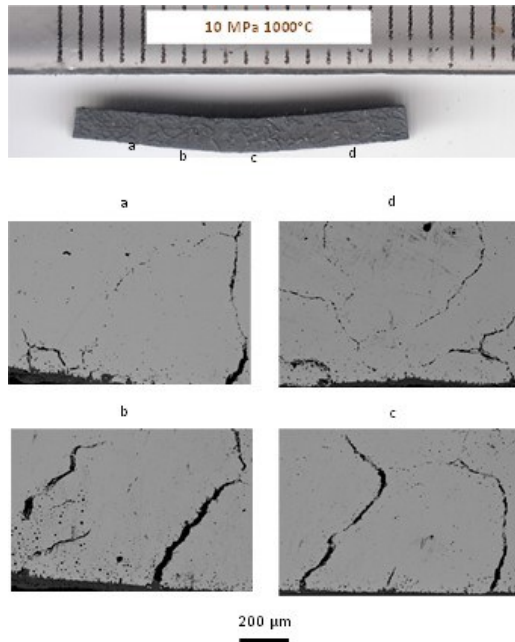


Fig. 3. The macrostructural analysis of the {10 MPa, 1000 °C}– specimen; illustration of its cracks–state

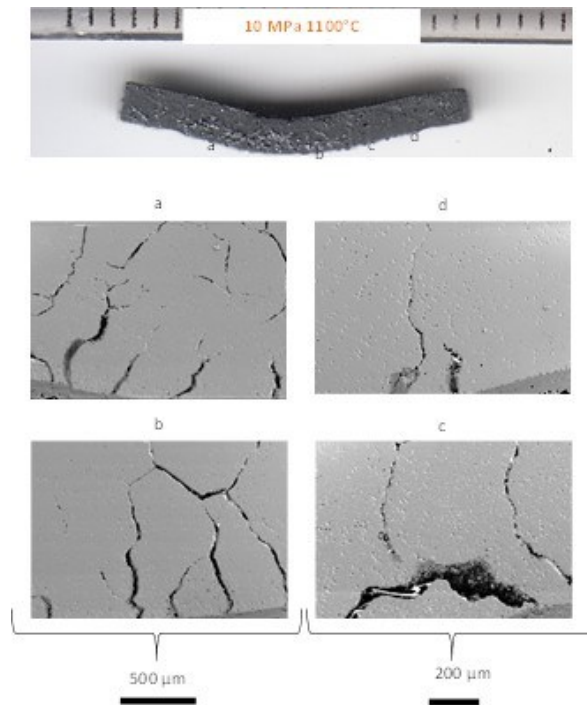


Fig. 4. The macrostructural analysis of the {10 MPa, 1100 °C}–crept specimen; illustration of its cracks–state

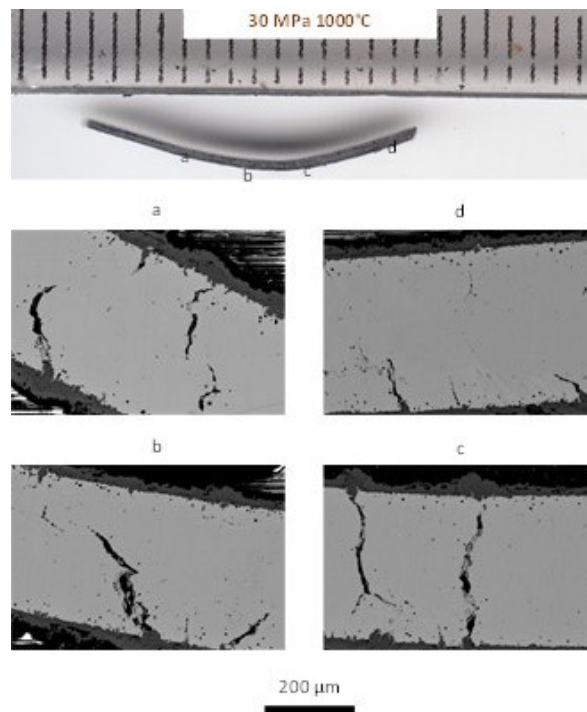


Fig. 5. The macrostructural analysis of the {30 MPa, 1000 °C}–crept specimen; illustration of its cracks–state

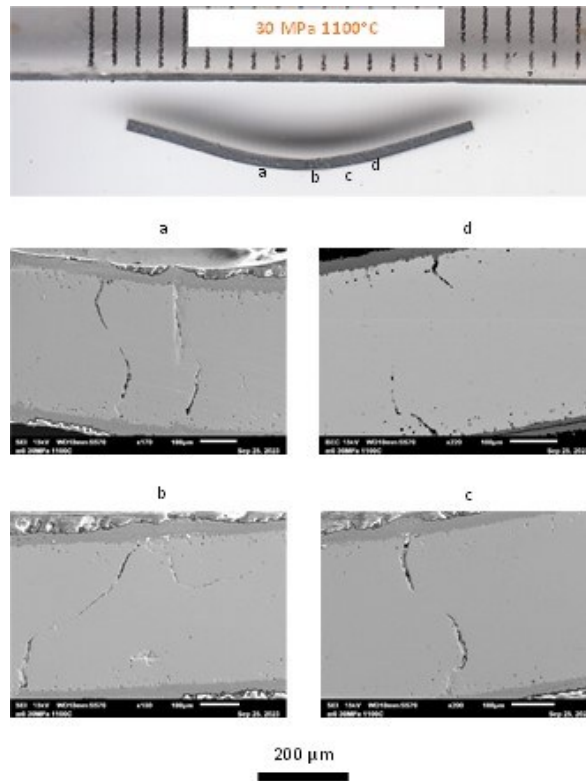


Fig. 6. The macrostructural analysis of the {30 MPa, 1100 °C}–crept specimen; illustration of its cracks–state

Oxidation states of the crept samples

During the creep tests the specimens were exposed to the impurities continuously conveyed and renewed by the flow of argon. This explains why the samples were so oxidized despite the very low content in oxygen (10 ppm). This exposure to hot oxidation was more or less longer than the real creep deformation since it was possible that the test was stopped later than the contact with the base. The real hot oxidation durations are given in the last column of Table 3. The four oxidation states are illustrated in Fig. 7, Fig. 8, Fig. 9 and Fig. 10.

Table 3. Values of the oxidation times for the four {σ,T} couples of conditions

(σ, T) couple of creep test conditions	Time to maximal deformation or to contact with base	Total duration of exposure to oxidation
10 MPa at 1000°C	149 h (def. ≈ 400μm)	149 h
10 MPa at 1100°C	99h (contact/base)	165 h
30 MPa at 1000°C	49h (contact/base)	63 h
30 MPa at 1100°C	5h (contact/base)	18 h

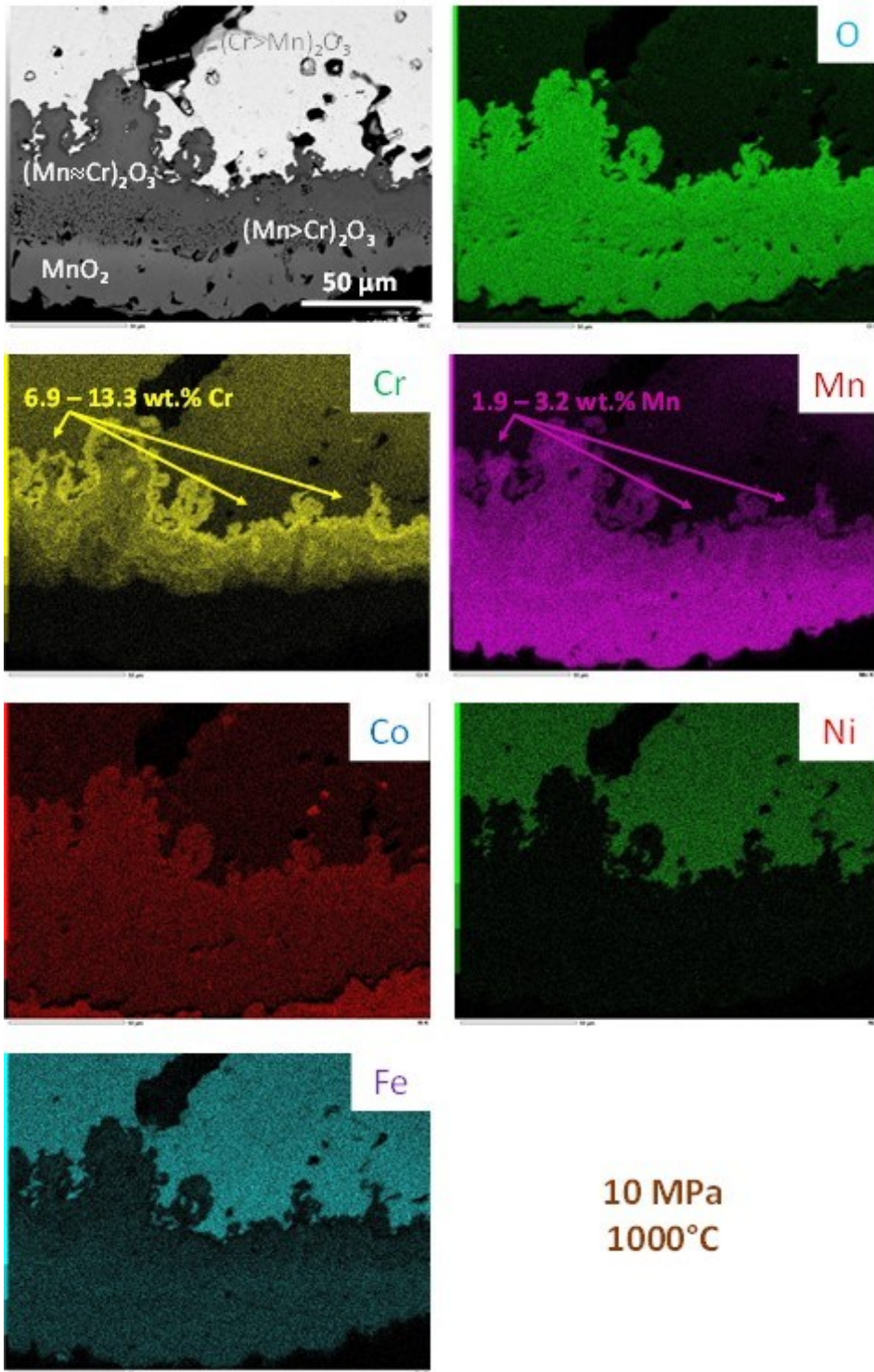


Fig. 7. SEM/BSE micrograph and EDS elemental mapping of the external oxide scale and of the deteriorated sub-surface of the {10 MPa, 1000 °C}-crept specimen

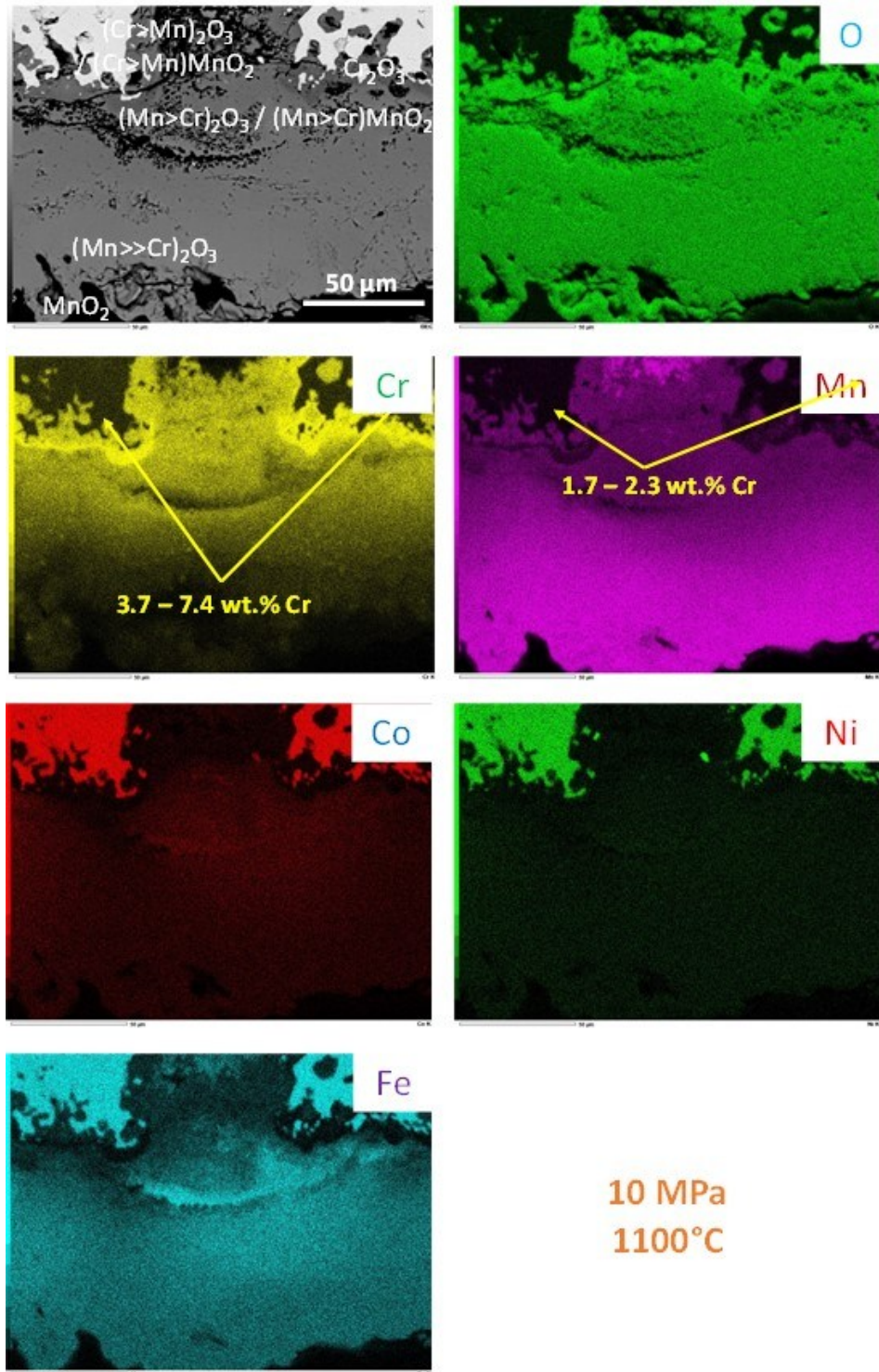


Fig. 8. SEM/BSE micrograph and EDS elemental mapping of the external oxide scale and of the deteriorated sub-surface of the {10 MPa, 1100 °C}-crept specimen

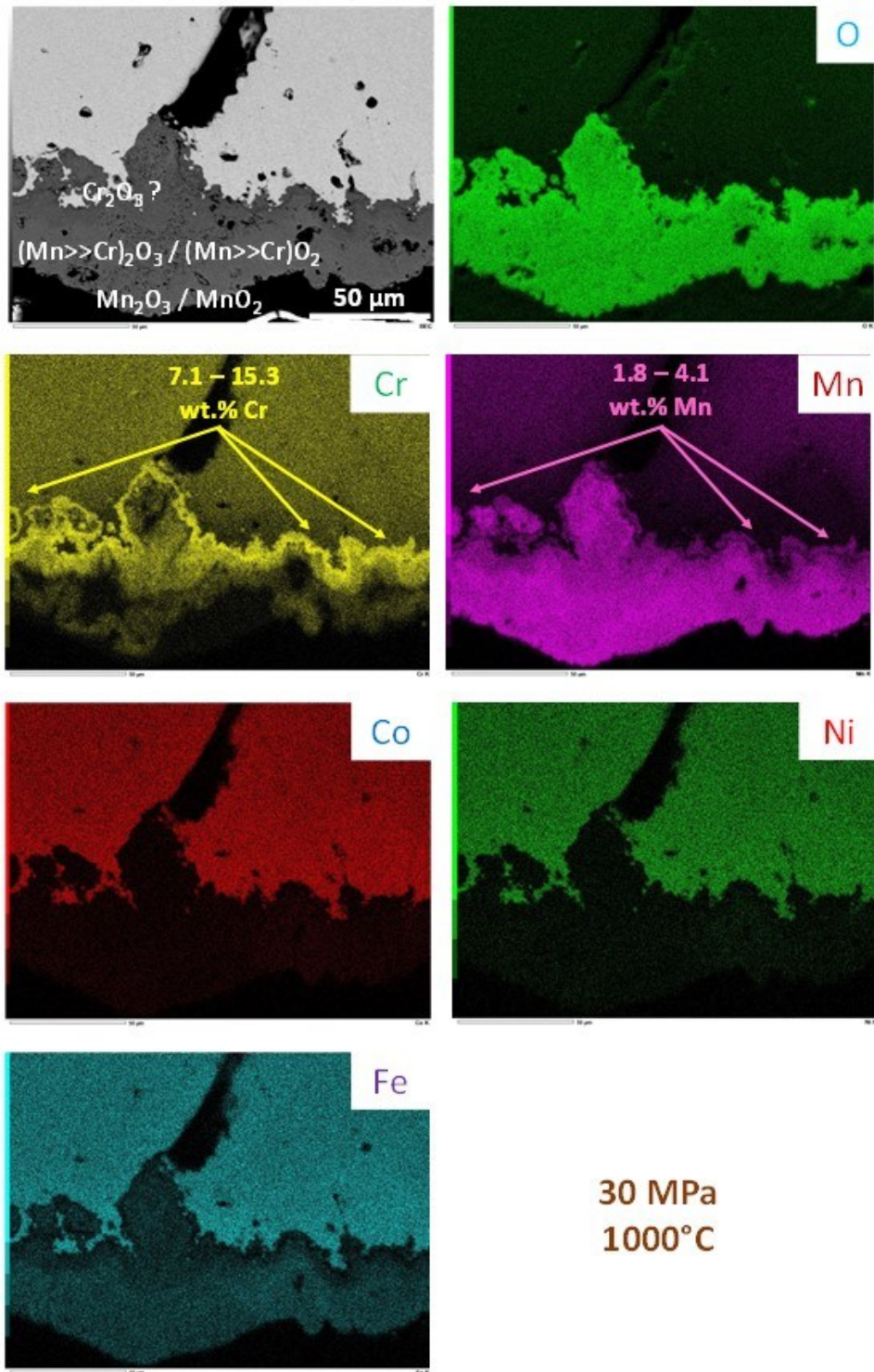


Fig. 9. SEM/BSE micrograph and EDS elemental mapping of the external oxide scale and of the deteriorated sub-surface of the {30 MPa, 1000 °C}-crept specimen

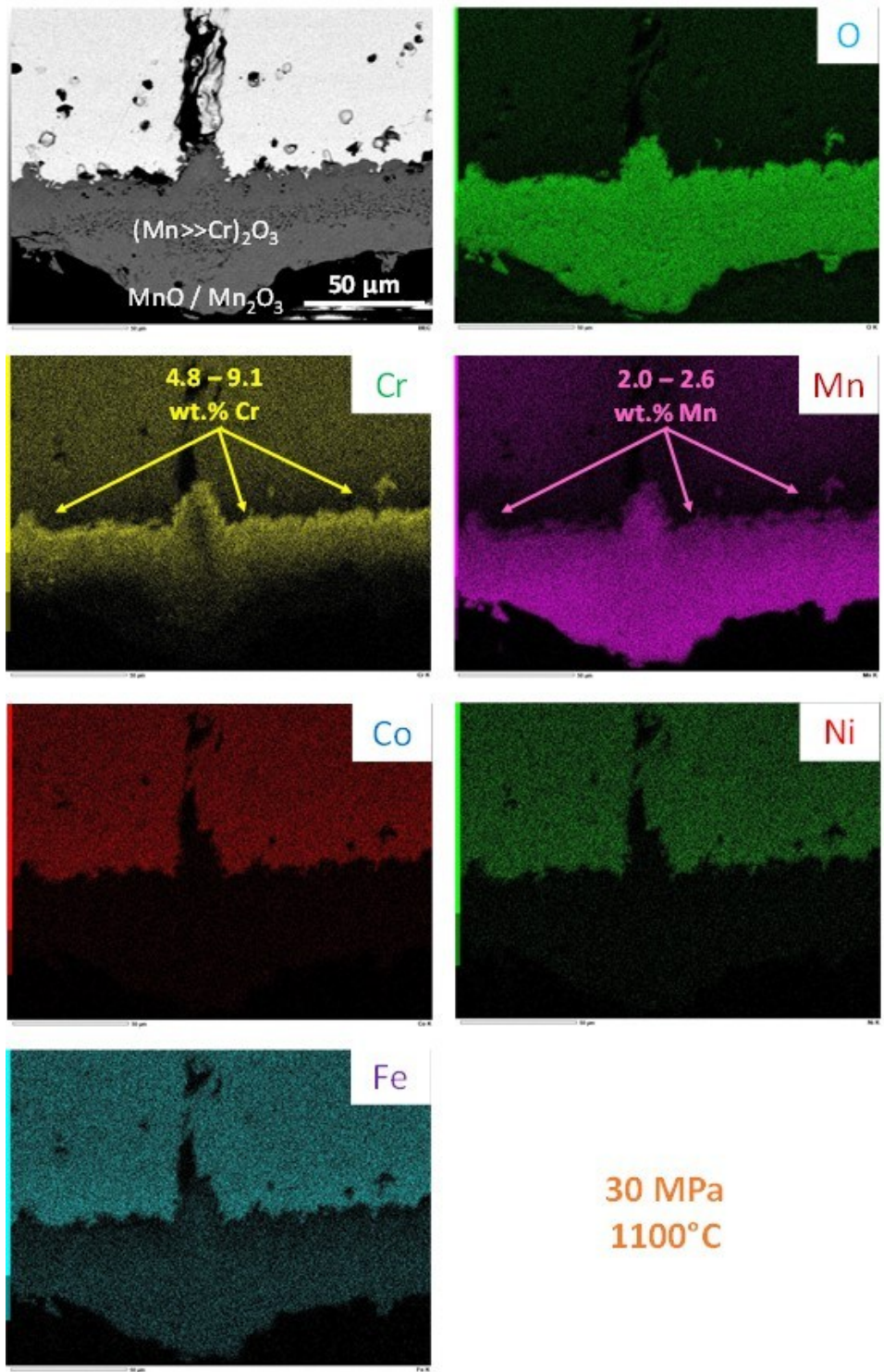


Fig. 10. SEM/BSE micrograph and EDS elemental mapping of the external oxide scale and of the deteriorated sub-surface of the {30 MPa, 1100 °C}-crept specimen

Oxidation by oxygen impurities obviously induced the development of external oxide scales. Their thickness is significant in all cases (50 to 150 μm) and depends on the (temperature, oxidation duration) conditions couple of the creep test: thickness increases with temperature and with oxidation duration. The EDS elemental maps show that these oxide scales are essentially rich in manganese and in chromium having quitted the alloy (sub-surfaces impoverished in Mn and Cr as evidenced by these same X-maps). Differences in signal intensity suggest that the oxide scales are poly-constituted. Beyond this qualitative information about the oxide nature, EDS spot analyses were carried out on each of the seen different parts of the scale (gray level more or less bright or dark). The quantitative results which were then obtained evidenced the stoichiometry of each type of oxide, or at least the relative importance of Mn and of Cr in the oxides. The results of this identification are given in the SEM/BSE micrograph in the top left part of Fig. 7 (resp. Fig. 8, Fig. 9 and Fig. 10) for the {10 MPa, 1000°C}-crept specimen (resp. {10 MPa, 1100°C}, {30 MPa, 1000°C} and {30 MPa, 1100°C}).

These results can be summarized as follows:

- * the complex {Mn, Cr}-oxides are richer and richer in oxygen from the interface between alloy and oxide scale to the interface of oxide scale and air,

- * the Mn content in oxide is higher and higher from the interface between alloy and oxide scale to the oxide scale / air interface,

- * the Cr content in oxide is lower and lower from the interface between alloy and oxide scale to the oxide scale / air interface.

For instance, chromium, or $(\text{Cr, Mn})_2\text{O}_3$ with Cr much more present than Mn, can be noticed close to the alloy, while $(\text{Mn, Cr})_2\text{O}_3$ with Mn much more present than Cr (and even MnO_2) is necessarily located in the outermost part of the oxide scale. Additional spot analyses were performed in the outermost part of the alloy to give some quantitative data concerning the impoverishment of Mn and Cr in the subsurface. The results are given in Figs. 7 to 10 as ranges of weight content variation in the X-maps corresponding to the Cr distribution and the Mn distribution. By comparison with the initial about 20 wt.% Cr and Mn contents (still existing deeper in the alloys), the results evidence a significant decrease in Cr and in Mn, particularly in Mn.

Discussion

One can point out first that the alloy was easy to elaborate by classical foundry. The targeted chemical composition was obtained – despite the high reactivity with oxygen of some elements (Cr and Mn) – thanks to the inert atmosphere produced by pumping and pure argon filling. It is also single-phased, as expected. However, as observed at the end of the creep tests for about 100 hours spent at high temperature in a constant flow of pure argon which contains oxygen traces, significant oxidation obviously took place. The formed external oxides, involving more Mn than Cr, are almost as thick as the alloys was exposed to air in the same conditions. This is due to the constant renewal of the oxygen traces induced by the flow of Ar.

Concerning the creep tests, the Cantor's alloy resistance is obviously too weak to represent any interest for long time service, under stress even of moderate level, at 1100°C but also at 1000°C. This was here demonstrated using a test mode which, unfortunately, cannot give data directly comparable to uniaxial creep tests. But the weakness of creep resistance showed by these results explain why published the results of mechanical tests obtained on the Cantor's alloy at really high temperature (namely $> 1000^\circ\text{C}$) – notably concerning the creep behavior – are so rare, almost inexistent in the literature. However, moderately interesting resistance was noted here at 1000°C for 10 MPa of maximal induced tensile stress. The intrinsic strength of this high entropy character of this alloy, well known for lower temperatures (down to ambient and cryogenic levels), seems acting here too, and for 10 MPa at 1000°C the alloy's resistance against creep deformation is not at all ridiculous taking into account that it does not benefit from strengthening precipitates (neither dispersed intermetallic compounds, nor secondary carbides, for example).

Observing the generalized cracks state affecting the crept samples available after these flexural creep tests highlights the necessity to reinforce grain boundaries (GB) along which cracks propagated. Among the possible GB-strengthening solutions one can think to eutectic refractory carbides, for instance. The same flexural creep test apparatus used in this work will be exploited again, this time on the carbides-strengthened versions of this alloy, allowing thus comparisons, with the present results. This should enable to value the expected progress realized in creep resistance. In case of success of the tested GB-strengthening solutions, creep tests – involving this time an uniaxial tensile creep test machine – will be scheduled to better know the creep behavior of the new alloys (with the determination of the constants involved in the equations of dependence on stress and on temperature) and to allow comparisons with results available in literature.

Conclusions

Until the present work, the creep behavior Cantor's alloy, equimolar in Co, Ni, Fe, Mn and Cr, was not investigated at temperatures beyond 1000°C, at least for general or local tensile stresses applied. The results obtained here allow understanding this lack of interest since this alloy is obviously much too weak, at least for its present equiaxed polycrystalline structure inherited from classical foundry. Acceptable creep resistance was noticed only for very moderate level of induced tensile stress (10 MPa). Nevertheless, it can be still considered for structural applications at high temperature, provided that it can be reinforced by strengthening atoms (W, Ta...) or particles (carbides), the presence of which will enrich the chemical composition beyond the current five elements.

These creep tests also gave information about the reactivity of such alloy, even in atmosphere extremely impoverished in oxygen, by pointing out the particular role of manganese. The rather fast oxidation, comparable to the behavior of such alloy in simple air, which was observed here highlights the deleterious effect of Mn which does not allow chromium playing its usual protective role. In parallel with the introduction of elements and phases devoted to enhance the creep resistance, another modification of the Cantor's alloy to consider for service at 1000°C and beyond is to remove manganese from its composition. Unfortunately, the suppression of Mn, which took part in the partial solving of the Ni and Co problem of critical elements, may be detrimental to the interest of such alloy in this field. Another element has then to be proposed for substituting Mn in this role.

Acknowledgment

The author would like to thank Lionel Aranda for his help in the creep tests.

References

- [1] Donachie, M. J. and Donachie, S. J. Eds., *Superalloys: a technical guide* (2nd ed.), United States, ASM International, 2002
- [2] Moroni, M., Rossetti, P., Naitza, S., Magnani, L., Ruggieri, G., Aquino, A., Tartarotti, P., Franklin, A., Ferrari, E., Castelli, D., Oggiano, G. and Secchi, F. *Factors controlling hydrothermal nickel and cobalt mineralization—Some suggestions from historical ore deposits in Italy*. **Minerals**, **9**, 429, pp. 1-41, 2019. <http://dx.doi.org/10.3390/min9070429>
- [3] Du, D., Yan, S., Yang, F., Zhu, Z., Song, Q. and Yang, Q. *Kriging interpolation for evaluating the mineral resources of cobalt-rich crusts on Magellan seamounts*. **Minerals**, **8**, 374, pp. 1-15, 2018. <http://dx.doi.org/10.3390/min8090374>
- [4] Dabrowa, J., Danielewski, M. *State-of-the-art diffusion studies in the high entropy alloys*. **Metals**, **10**, pp. 1–44, 2020. <https://doi.org/10.3390/met10030347>

- [5] Cantor, B., Chang, I. T., Knight, P., Vincent, A. J. *Microstructural development in equiatomic multicomponent alloys*. **Materials Science & Engineering A**, **375-377**, pp. 213–218, 2004. <https://doi.org/10.1016/j.msea.2003.10.257>
- [6] Yeh, J. W., Chen, S. K., Lin, S. J., Gan, J. Y., Chin, T. S., Shun, T. T., Tsau, C. H. and Chang, S. Y. *Microstructural development in equiatomic multicomponent alloys*. **Advanced Engineering Materials**, **6**, pp. 299–303, 2004. <https://doi.org/10.1002/adem.200300567>
- [7] Wang, Z., Guo S., Wang, Q., Liu, Z., Wang, J., Yang, Y. and Liu, C. T. *Nanoindentation characterized initial creep behavior of a high-entropy-based alloy CoFeNi*. **Intermetallics**, **53**, pp. 183–186, 2014. <http://dx.doi.org/10.1016/j.intermet.2014.05.007>
- [8] Bahadur, F., Kumar, J., Gururaj, K., Kumar Yadav, M., Tan S., Pradeep, K. G., Gurao, N. P. and Biswas, K. *Room temperature cyclic creep behaviour of equimolar CoCuFeMnNi high entropy alloy*. **Materials Science & Engineering A**, **865**, 144587, 2023. <https://doi.org/10.1016/j.msea.2023.144587>
- [9] Tsao T. K., Yeh A. C., Kuo C. M., Kakehi K., Murakami H., Yeh J. W. and Jian S. R. *The high temperature tensile and creep behaviors of high entropy superalloy*. **Scientific Reports**, **7**, 12658, 2017. <https://doi.org/10.1038/s41598-017-13026-7>
- [10] Chen, S., Qiao, J., Diao, H., Yang, T., Poplawsky, J., Li, W., Meng, F., Tong, Y., Jiang, L., Liaw, P. K. and Gao, Y. *Extraordinary creep resistance in a non-equiatomic high-entropy alloy from the optimum solid-solution strengthening and stress-assisted precipitation process*. **Acta Materialia**, **244**, 118600, 2023. <https://doi.org/10.1016/j.actamat.2022.118600>
- [11] Lee, D. H., Seok, M. Y., Zhao, Y., Choi, I. C., He, J., Lu, Z., Suh, J. Y., Ramamurty, U., Kawasaki, M., Langdon, T. G. and Jang, J. I. *Spherical nanoindentation creep behavior of nanocrystalline and coarse-grained CoCrFeMnNi high-entropy alloys*. **Acta Materialia**, **109**, pp. 314–322, 2016. <http://dx.doi.org/10.1016/j.actamat.2016.02.049>
- [12] Xu, Z., Zhang, H., Li, W., Mao, A., Wang, L., Song, G. and He, Y. *Microstructure and nanoindentation creep behavior of CoCrFeMnNi high entropy alloy fabricated by selective laser melting*. **Additive Manufacturing**, **28**, pp. 766–771, 2019. <https://doi.org/10.1016/j.addma.2019.06.012>
- [13] Kumar, J., Linda, A., Sadhasivam, M., Pradeep, K. G., Gurao, N. P. and Biswas, K. *The effect of Al addition on solid solution strengthening in CoCrFeMnNi: Experiment and modelling*. **Acta Materialia**, **238**, 118208, 2022. <https://doi.org/10.1016/j.actamat.2022.118208>
- [14] Jing, Q., Hu, L., Li, J., Xin, S., Huang, S. and Liu, L. *Significant strength enhancement of high-entropy alloy via phase engineering and lattice distortion*. **Journal of Alloys and Compounds**, **976**, 172963, 2024. <https://doi.org/10.1016/j.jallcom.2023.172963>
- [15] Shams, S. A. A., Jang, G., Won, J. W., Bae, J. W., Jin, H., Kim, H. S. and Lee, C. S. *Low-cycle fatigue properties of CoCrFeMnNi high-entropy alloy compared with its conventional counterparts*. **Materials Science & Engineering A**, **792**, 139661, 2020. <https://doi.org/10.1016/j.msea.2020.139661>
- [16] Hao, R., Wang, Z., Jin, X., Lan, A. and Qiao, J. *A flow model in CoCrFeMnNi high-entropy alloys during high-temperature tension*. **Applied Physics Letters**, **124**, 101902, 2024. <https://doi.org/10.1063/5.0191459>
- [17] Kim, Y. K., Lim, K. R. and Lee, K. A. *Superior resistance to high-temperature creep in an additively manufactured precipitation-hardened CrMnFeCoNi high-entropy alloy nanocomposite*. **Materials & Design**, **227**, 111761, 2023. <https://doi.org/10.1016/j.matdes.2023.111761>

- [18] Kim, Y. K., Yang, S. and Lee, K. A. *Compressive creep behavior of selective laser melted CoCrFeMnNi high entropy alloy strengthened by in-situ formation of nano-oxides. Additive Manufacturing*, **36**, 101543, 2020. <https://doi.org/10.1016/j.addma.2020.101543>
- [19] Rozman, K. A., Detrois, M., Liu, T., Gao, M. C., Jablonski, P. D. and Hawk, J. A. *Long-term creep behavior of a CoCrFeNiMn high-entropy alloy. Journal of Materials Engineering and Performance*, **29(9)**, pp. 5822-5839, 2020. <https://doi.org/10.1007/s11665-020-05103-2>
- [20] Song, C., Li, G., Li, G., Zhang, G. and Cai, B. *Tensile creep behavior and mechanism of CoCrFeMnNi high entropy alloy. Micron*, **150**, 103144, 2021. <https://doi.org/10.1016/j.micron.2021.103144>
- [21] Lee, K. H., Hong, S. K. and Hong, S. I. *Precipitation and decomposition in CoCrFeMnNi high entropy alloy at intermediate temperatures under creep conditions. Materialia*, **8**, 100445, 2019. <https://doi.org/10.1016/j.mtla.2019.100445>
- [22] Jeong, H. T., Park, H. K., Park, K., Na, T. W. and Kim, W. J. *High-temperature deformation mechanisms and processing maps of equiatomic CoCrFeMnNi high-entropy alloy. Materials Science & Engineering A*, **756**, pp. 528–537, 2019. <https://doi.org/10.1016/j.msea.2019.04.057>
- [23] Gholizadeh, R., Yoshida, S., Bai, Y., Kurokawa, S., Shibata, A. and Tsuji, N. *Global understanding of deformation behavior in CoCrFeMnNi high entropy alloy under high-strain torsion deformation at a wide range of elevated temperatures. Acta Materialia*, **243**, 118514, 2023. <https://doi.org/10.1016/j.actamat.2022.118514>
- [24] Gadelmeier, C., Agudo Jacome, L., Suarez Ocano, P., and Glatzel, U. *Effect of stacking fault energy (SFE) of single crystal, equiatomic CrCoNi and Cantor alloy on creep resistance. Effect of stacking fault energy (SFE) of single crystal, equiatomic CrCoNi and Cantor alloy on creep resistance. Materials Science & Engineering, A* **908**, 146779, 2024. <https://doi.org/10.1016/j.msea.2024.146779>

Received: October 14, 2024

Accepted: November 28, 2024